Supplemental Material: The effects of inhomogeneities on scroll-wave dynamics in an anatomically realistic mathematical model for canine ventricular tissue

K. V. Rajany[a,1,*], Rupamanjari Majumder[b], Alok Ranjan Nayak[c], Rahul Pandit[d,2]

[a]*Centre for Condensed Matter Theory, Department of Physics, Indian Institute of Science, Bangalore 560012, India.*
[b]*Department of Fluid Dynamics, Pattern Formation and Biocomplexity, Max Planck Institute for Dynamics and Self-Organization.*
[c]*International Institute of Information Technology, Bhubaneswar.*
[d]*Centre for Condensed Matter Theory, Department of Physics, Indian Institute of Science, Bangalore 560012, India.*

Abstract

In this Supplementary Material we give (a) details of the numerical methods we use to obtain the results in the main part of this paper (Section I), (b) links to the videos that illustrate the spatiotemporal evolution of the transmembrane potential for Figs. (3), (4), (5), (6), (7), and (8) in the main paper(Section II) and (c), the Hund-Rudy-Dynamic(HRD) cell model (Section III), and a few important plots from the cell model simulations, viz, APDR curves, AP curves, frequency of the scroll waves etc.

1. Numerical Methods

In our direct numerical simulations (DNSs), we consider monodomain tissue. We solve a reaction-diffusion-type partial differential equation (PDE), in which the diffusion tensor is determined by the fiber-orientation directions:

$$\frac{\partial V}{\partial t} = \nabla \cdot D \nabla V - \frac{(I_{ion} + I_{applied})}{C_m}, \tag{1}$$

where V is the transmembrane voltage, D is the diffusion tensor (see below) that describes the diffusion of the voltage through the medium, I_{ion} is the sum of all the ionic currents, $I_{applied}$ is the external stimulus, and C_m is the membrane capacitance per unit area.

The action potential (AP) propagates faster in the direction parallel to the muscle fibers than in the direction perpendicular to them. This property is taken into account in our calculations by defining the local conductivity tensor D_{ij}, which is derived from the local fiber direction, as follows:

$$D_{ij} = D_{\|}\delta_{ij} + (D_{parallel} - D_{\perp})\alpha_i\alpha_j, \tag{2}$$

where α is the vector describing muscle fiber direction, and $D_{\|}$ and $D_{\perp}$ are the conductivities in the longitudinal and transverse fiber directions, respectively. The ratio $D_{\|} : D_{\perp} = 4 : 1$, which is comparable to the experimentally recorded ratios.

We assume that the transverse conductivity is the same in directions orthogonal to the muscle-fiber direction.

*Corresponding author
Email addresses: rajanyk@iisc.ac.in (K. V. Rajany), rahul@iisc.ac.in (Rahul Pandit)
[1]Present address:S.A.R.B.T.M. Govt. College, Koyilandy, Calicut, India
[2]also at Jawaharlal Nehru Centre For Advanced Scientific Research, Jakkur, Bangalore, India.

Table 1: Table showing, for our DNSs, the size of the simulation domain, the space and time steps (δx and δt), the real-time equivalent of the duration of the simulation (T).

DNS	Domain size	δx	δt	T
$3D - HRD$	$416 \times 416 \times 416$	0.02	0.02	3s

Figure 1: Two level isosurface plots (at four representative times, which increase from left to right) of the transmembrane potential V showing how a scroll wave is formed and how it develops, in the anatomical dog-heart geometry after we apply the S1-S2 cross-field stimuli (see text). For the complete spatiotemporal evolution see the Video S31

We use a finite-difference method for computing the spatial evolution; and we employ the forward-Euler scheme for computing the temporal evolution of the system. We use no-flux boundary conditions at the borders. Boundary conditions are handled by the *phase-field method*.

The size of the domain, the space step and time steps that we use in our DNSs (δx and δt), the real-time equivalent of the simulation(T) and the total run-time of the program(τ_{tot}) for each of our DNSs are given in Table 1. These DNSs are computationally intensive. The programs are run on a CRAY supercomputer by using 6656 processors for the 3D heart simulations.For each parameter set we used 416 processors. We had 28 parameter sets. We used $16 \times 416 = 6656$ processors for simultaneously running the 16 parameter sets.

The size of the large-scale localized inhomogeneity that we used in this study is $\sim 12mm$ and the small-scale distributed inhomogeneities are of size $\sim 2mm$.

We have also developed a combined MPI-CUDA program for our computations; we have run these on CPU-GPU hybrid computer systems and thus achieved great improvement in computational performance. The 416 cores that we use on a CRAY computer system requires 8 hours to simulate the real-time equivalent of 3 seconds, for a single parameter value. Our MPI-CUDA implementation needs almost the same time with 24 cores; each CPU core is attached to one GPU; thus, we use a total of 24 CPUs and 24 GPUs in our MPI-CUDA program.

For our 3D simulation we use the processed Diffusion-Tensor Magnetic-Resonance Imaging (DTMRI) data for the canine-ventricular anatomy, which is freely available for academic purposes at the CMISS website (https://www.cmiss.org/). This geometry, of a structurally normal canine heart, has been obtained via DTMRI, which is a non-invasive technique, based on measuring the Brownian motion of water molecules in anisotropic cardiac tissue; this motion is constrained by the tissue structure. It shows only grey-scale images. Typically, images are obtained in tissue slices; and then these images are assembled into a 3D volume. The image contains the Cartesian coordinates of the points within the heart and the direction cosines of the orientation of the muscle fiber at each point. For our 3D DNSs, we place this geometry inside a cube of side 8.32 cm. The simulation domain consists of a total of around 72 million grid points.

We use the S1-S2 cross-field protocol to initiate scroll waves in the medium. In this protocol, we begin with a plane wave S1, which is initiated from one end. When it has passed through half the medium, we apply a cross field, i.e., another plane wave in the perpendicular direction (the S2 stimulus). This creates a scroll wave in the 3D geometry, which we use as an initial condition. Figure 1 shows the development of the initial scroll that we obtain by using the S1-S2 protocol. $D_{\|}$ in Eq.2 is $2cm^2/s$ for the HRD model.

1.1. The Phase-field method for the imposition of Boundary Conditions in Anatomical Geometries

In our numerical simulations we use no-flux boundary conditions. In conventional methods, we need to track the boundaries and calculate the normal to the surface at each point; this is computationally costly. The phase-field method, proposed by Fenton *et al.* [1], uses a different approach in which the boundary between the cardiac muscle and the surrounding medium is converted into a smooth, spatially diffuse interface of small thickness for a *phase* variable ϕ.

The boundary conditions for the heart wall: there is zero current flow normal to the tissue boundary surfaces, so

$$\hat{n}.D\nabla V = 0, \tag{3}$$

where $\hat{n}$ is the unit vector normal to the heart surface. We now define a phase variable ϕ, that takes different values inside and outside of the heart tissue and varies smoothly across a thin, diffuse interface between them: $\phi = 1$ inside the heart and $\phi = 0$ outside the heart. To calculate ϕ in the interfacial region we solve the following equation:

$$\frac{\partial \phi}{\partial t} = \zeta^2 \nabla^2 \phi - \frac{\partial G(\phi)}{\partial \phi}, \tag{4}$$

where ζ controls the width of the interface. $G(\phi)$ is a function of the form of a double-well potential with minima at $\phi = 0$ and $\phi = 1$.

$$G(\phi) = -\frac{(2\phi - 1)^2}{4} + \frac{(2\phi - 1)^4}{8}. \tag{5}$$

We use a time step of $\delta t = 0.01$ ms and a space step of $\delta x = 0.025$ cm . The phase profile of ϕ is used to interpolate smoothly the properties of the interior and exterior regions. The variables now change as follows: $C_m \to \phi C_m, I_{ion} \to \phi I_{ion}$, and $\sigma \to \phi\sigma$, respectively. The reaction-diffusion equation then assumes the following form:

$$\phi \frac{\partial V}{\partial t} = \nabla.[D\phi\nabla V] - \phi \frac{I_{ion}}{C_m}. \tag{6}$$

No calculations are carried out where $\phi = 0$. We set $\phi = 0$ below the cut-off value of $\phi = 1 \times 10^{-4}$. This saves computational time, but does not affect our numerical results significantly.

2. Cell level Plots and other important plots

3. Movies showing the spatiotemporal evolution of the various systems in this study

This section contains the links to the movies of the two-level isosurface plots of the transmembrane potential V illustrating the spatiotemporal evolution of scroll waves in the HRD model, in the anatomically realistic geometry for a canine ventricle, with and without inhomogeneities. These movies correspond to the Figs. (3)-(8) in the main paper.

Supporting Information

Videos are hyperlinked.
Please click on Video "S#", which is bounded by a rectangular box, to play the video;
here # denotes the number of the video.
The videos should play with VLC Media Player.

Without any inhomogeneities.

We use two different parameter sets: the first yields a rotating scroll wave; and the second gives broken scroll waves interacting with each other.

Video S41:
Video S42:

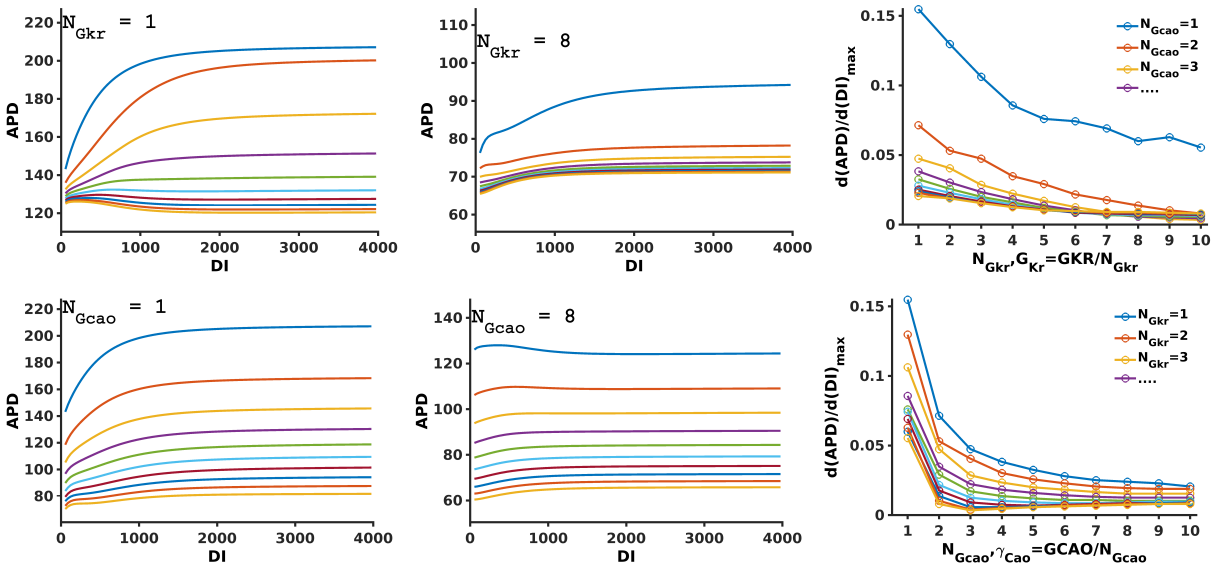

Figure 2: Plots for the HRD model of the APD restitution (APDR) curves for 3 representative parameter sets in each row; the diastolic interval (DI) is on the horizontal axis; and the vertical axis shows the corresponding value of the APD. Top panel: the variation of the APDR with N_{GCao}, for 3 fixed values of N_{GKr}; bottom panel: the variation of the APDR with N_{GKr}, for 3 fixed values of N_{GCao}. On the right sides of these plots, we depict the corresponding plots for the maximal values of the slopes($d(APD)/d(DI)$) of the restitution curves. The maximal slopes decrease with an increase in N_{GKr} as well as with a decrease in γ_{Cao}. We show later that the flat-slope region gives rise to stable rotating spiral and scroll waves in 2D tissue and in the 3D geometry, respectively.

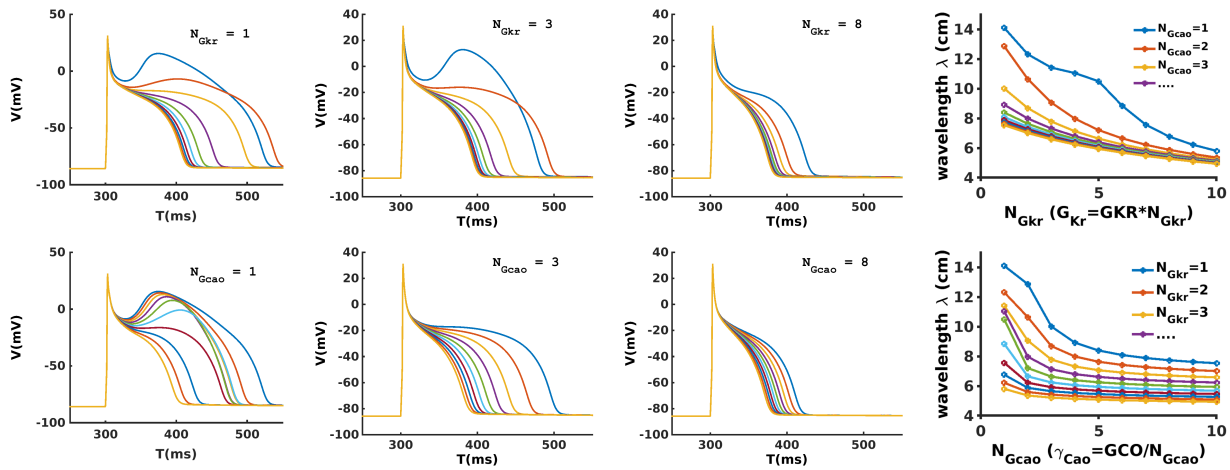

Figure 3: Plots of the transmembrane potential V versus time illustrating the variation of the shape of the action potential (AP) as we change (a) γ_{Cao}, while G_{Kr} is held constant (top panel), and (b) G_{Kr}, for a fixed value of γ_{Cao} (bottom panel), in the HRD model, for 3 representative cases. The wavelength $\lambda = APD \times cv$, where cv is the conduction velocity and APD is the AP duration (see text). On the right side, we show these wavelengths for all the 10×10 combinations.

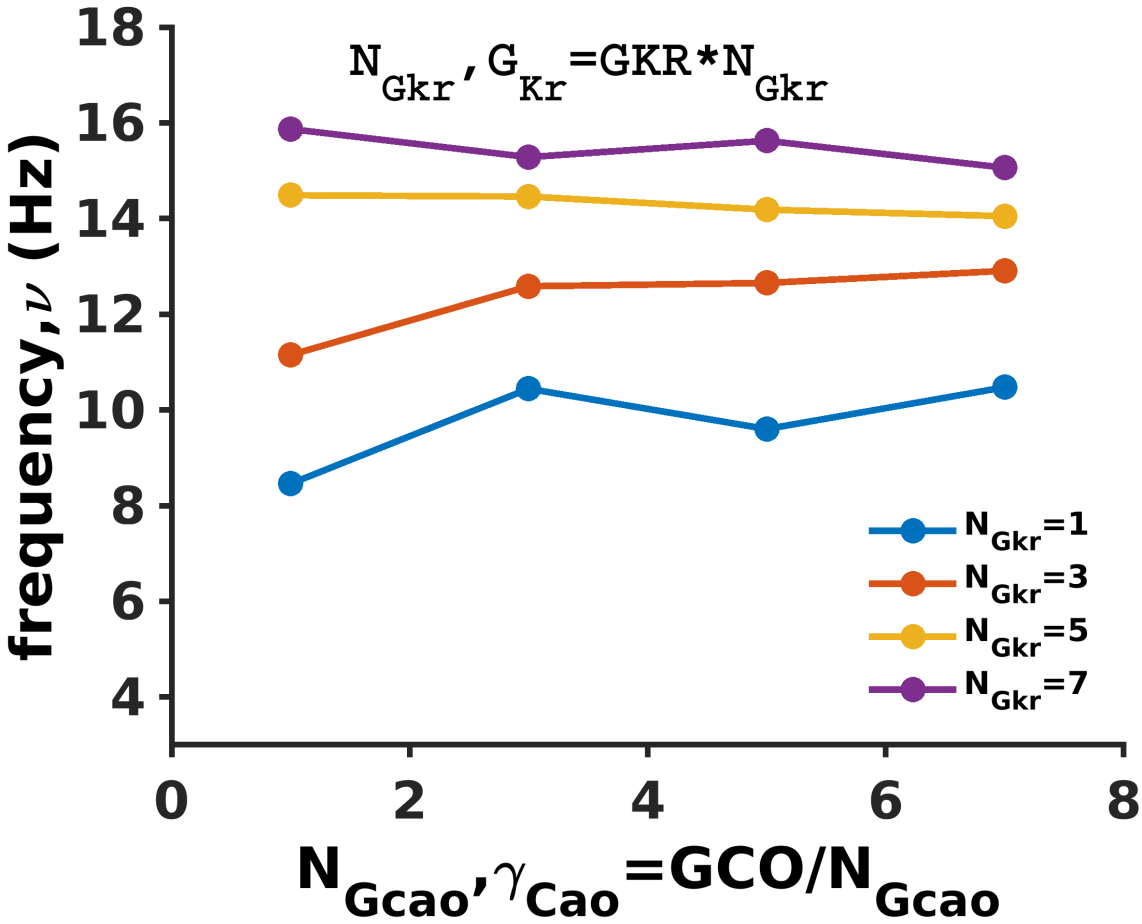

Figure 4: The dominant frequencies that we obtain from power spectra for all our parameter values, i.e., for $N_{GKr} = 1, 2..7$ and $N_{GCao} = 1, 2..7$. In the region where stable rotating waves exist, we see a prominent frequency in the spectrum. If the waves are unstable and disappear, it is not possible to identify a major frequency.

When a medium-sized spherical inhomogeneity of conduction type is placed at four different positions.

Position 1 with a broken-wave initial condition:
Video S43:
Position 2 with a broken-wave initial condition:
Video S44:
Position 3 with a broken-wave initial condition:
Video S45:
Position 4 with a broken-wave initial condition:
Video S46:
Position 1 with rotating-wave initial condition:
Video S47:
Position 2 with a rotating-wave initial condition:
Video S48:
Position 3 with a rotating-wave initial condition:
Video S49:
Position 4 with a rotating-wave initial condition:
Video S410:

With small conduction inhomogeneities distributed in the domain for three different concentrations of the inhomogeneities

5% inhomogeneities with the broken-scroll-state initial condition:
Video S411:
10% inhomogeneities with the broken-scroll-state initial condition:
Video S412:
20% inhomogeneities with the broken-scroll-state initial condition:
Video S413:
5% inhomogeneities with the rotating-scroll-state initial condition:
Video S414:
10% inhomogeneities with the rotating-scroll-state initial condition:
Video S415:
20% inhomogeneities with the rotating-scroll-state initial condition:
Video S416:

With a medium-sized spherical inhomogeneity, of ionic type, is placed at four different positions.

Position 1 with the broken-scroll-state initial condition:
Video S417:
Position 2 with the broken-scroll-state initial condition:
Video S418:
Position 3 with the broken-scroll-state initial condition:
Video S419:
Position 4 with the broken-scroll-state initial condition:
Video S420:
Position 1 with the rotating-scroll-state initial condition:
Video S421:
Position 2 with the rotating-scroll-state initial condition:
Video S422:
Position 3 with the rotating-scroll-state initial condition:
Video S423:
Position 4 with the rotating-scroll-state initial condition:
Video S424:

With small ionic inhomogeneities are distributed in the domain with three different concentrations

5% inhomogeneities with the rotating-scroll-state initial condition:
Video S425:
10% inhomogeneities with the rotating-scroll-state initial condition:
Video S426:
20% inhomogeneities with the rotating-scroll-state initial condition:
Video S427:
5% inhomogeneities with the broken-scroll-state initial condition:
Video S428:
10% inhomogeneities with the broken-scroll-state initial condition:
Video S429:
20% inhomogeneities with the broken-scroll-state initial condition:
Video S430:

4. Formulation of the Hund-Rudy-Dynamic (HRD) Cell Model

The complete HRD-model equations are described below.

Abbreviations and Definitions

Table 2: **General Parameters**

Abbreviation	*Definition*	*Unit*
V_m	Membrane voltage	mV
E_x	Reversal potential of current x	mV
$\bar{I}_x$	Maximum current carried through the channel, x	$\mu A/\mu F$
$\overline{G}_x$	Maximum conductance of the channel, x	$ms/\mu F$
X_∞	Steady state value of variable X	
X_τ	Time constant of variable X	
α_y, β_y	Opening and closing rate constants of gate y, respectively.	
P_S	Membrane permeability to ion S	cm/s
$P_{S,A}$	Permeability ratio of ion S to ion A	
γ_S	Activity coefficient of ion S	cm/s
z_s	Valence of ion S	
V_X	Volume of Compartment X	
R	Gas constant, 8314 J/kmol/K	
T	Temperature, 310	K
F	Faraday constant, 96487.	C/mol
C_m	Total cellular membrane capacitance, 1	μF
A_{Cap}	Capacitative membrane area	cm^2
A_{Geo}	Geometric membrane area	cm^2
R_{CG}	Ratio of A_{Cap} to A_{Geo} = 2.	

Table 3: **Currents, Pumps and Exchangers**

Abbreviation	*Definition*	*Unit*
I_{Na}	Fast Na^+ current	$\mu A/\mu F$
$I_{Na,L}$	Slowly inactivating late Na^+ current	$\mu A/\mu F$
$I_{Na,b}$	Background Na^+ current	$\mu A/\mu F$
I_{CaL}	Ca^{2+} current through the L-type Ca^{2+} channel	$\mu A/\mu F$
$I_{Ca,b}$	Background Ca^{2+} current	$\mu A/\mu F$
$I_{p,Ca}$	Sarcolemmal Ca^{2+} current	$\mu A/\mu F$
I_{CaNa}	Na^+ current through the L-type Ca^{2+} channel	$\mu A/\mu F$
I_{CaK}	K^+ current through the L-type Ca^{2+} channel	$\mu A/\mu F$
I_{Kr}	Rapid delayed rectifier K^+ current	$\mu A/\mu F$
I_{Ks}	Slow delayed rectifier K^+ current	$\mu A/\mu F$
I_{to1}	4AP-sensitive transient outward K^+ current	$\mu A/\mu F$
I_{to2}	Ca^{2+} dependent transient outward Cl^- current	$\mu A/\mu F$
I_{K1}	Time-independent K^+ current	$\mu A/\mu F$
I_{Kp}	Plateau K^+ current	$\mu A/\mu F$
$I_{Cl,b}$	Background Cl^{2+} current	$\mu A/\mu F$
I_{NaCa}	Na^+ - Ca^- current	$\mu A/\mu F$
I_{NaK}	Na^+ - K^+ pump	$\mu A/\mu F$
I_{pCa}	Sarcolemmal Ca^{2+} pump	$\mu A/\mu F$
CT_{NaCl}	Na^+ -Cl^- cotransporter	mmol/L per ms
CT_{KCl}	K^+ -Cl^- cotransporter	mmol/L per ms
$I_{Ca,t}$	Total transmembrane Ca^{2+} current $I_{Ca,t} = I^{Ca,L} + I_{Ca,b} + I_{p,Ca} - 2I_{Na,Ca}$	
$I_{Na,t}$	Total transmembrane Na^+ current $I_{Na,t} = I_{Na} + 3I_{NaK} + 3I_{NaCa} + I_{NaL} + I_{Nab}$	
$I_{K,t}$	Total transmembrane K^+ current $I_{K,t} = I_{Ks} + I_{Kr} + I_{K1} + I_{to1} + I_{Kp} - 2I_{NaK}$	
$I_{Cl,t}$	Total transmembrane Cl. current $I_{Cl,t} = I_{to2} + I_{Clb}$	
I_{tot}	Total transmembrane current $I_{tot} = I_{Ca,t} + I_{Na,t} + I_{K,t} + I_{Cl,t}$	
I_{stim}	Stimulus current	$\mu A/\mu F$
ACT	I_{CaL} activation parameter	
α	I_{CaL} Rate Constant, activation	
β	I_{CaL} Rate Constant, deactivation	
C	I_{CaL} State, closed (Ca^{2+} free)	
O	I_{CaL} State, open (Ca^{2+} free)	
I_V	I_{CaL} inactivation parameter (Ca^{2+} free)	
x	I_{CaL} Rate Constant, recovery from inactivation (Ca^{2+} free)	
y	I_{CaL} Rate Constant, inactivation (Ca^{2+} free)	
CI	I_{CaL} State closed state, inactivation (Ca^{2+} free)	
OI	I_{CaL} State open state, inactivation (Ca^{2+} free)	
Allo	Ca^{2+} dependent allosteric activation factor of I_{NaCa}	
ν_{max}	Maximal flux of I_{NaCa}	
k_{sat}	Saturation factor of I_{NaCa} at negative potentials	
η	Position of energy barrier of I_{NaCa}	
f_{NaK}	Voltage dependent parameter of I_{NaK}	
σ	$[Na^+]_o$ -dependent factor of f NaK	
$I_{p,Ca}$	Sarcolemmal Ca^{2+} pump	$\mu A/\mu F$

$I_{Ca,b}$	Background Ca^{2+} current	$\mu A/\mu F$
CT_{NaCl}	Na^+ - Cl^- cotransporter	mmol/L per ms
CT_{KCl}	K^+ -Cl^- cotransporter	mmol/L per ms
τ_{ri}	Time constant of I_{rel} inactivation	ms
τ_{diff}	Time constant of Ca^{2+} transfer from SS to myoplasm	ms
APD	Action potential duration measured at 90% repolarization	
CaT	Calcium transient	
CaT_{amp}	Calcium transient amplitude	
PLB	Phospholamban	
RyR	Ryanodine receptor SR Ca^{2+} release channel	
LTCC	L-type Ca^{2+} channel	
K_m	Half-saturation concentration	mmol/L
m, h, and j	Activation gate, fast inactivation gate, and slow inactivation gate of I_{Na}, respectively.	
m_L and h_L	Activation gate and inactivation gate of I_{NaL}, respectively	
d, f, and f_2	Activation gate, fast voltage-dependent inactivation gate, and slow voltage-dependent inactivation gate of I_{CaL}, respectively.	
poww	Power applied to d	
$f_{Ca}$and f_{Ca2}	Fast Ca^{2+} -dependent inactivation gate and slow Ca^{2+} -dependent inactivation gate of I_{CaL}, respectively.	
$X_{s1}$and X_{s2}	Fast activation gate and slow activation gate of I_{Ks}, respectively	
X_r	Activation gate of I_{Kr}	
R_{Kr}	Time-independent rectification gate of I_{Kr}	
K_1	Inactivation gate of I_{K1}	
a, i, i 2	Activation gate, fast inactivation gate, and slow inactivation gate of I_{to1} , respectively	
R_{to1}	time-independent rectification gate of I_{to1}	
AA	Ca^{2+} -dependent activation gate of I_{to2}	
ro and ri	Activation gate and inactivation gate of I_{rel} , respectively.	
Δro_∞	JSR Modulation of ro_∞ by $[Ca^{2+}]$ JSR	
vg	Variable gain factor for I_{rel}	
y_∞	Steady-state value of gate y	
$\alpha_y$and β_y	Opening and closing rate constants of gate y, respectively	ms^{-1}
τ_y	Time constant of gate y	ms
$\bar{I}_x$	Maximum current carried through channel x	$\mu A/\mu F$
$\Delta[S]_x$	Change in concentration of ion S in compartment x during one time step	mmol/L

Table 4: **Ionic Fluxes and Diffusion**

I_{rel}	Ca^{2+} release from JSR to myoplasm	mmol/L per ms

I_{up}	Ca^{2+} uptake from myoplasm to NSR	mmol/L per ms
I_{leak}	Ca^{2+} leak from JSR to myoplasm	mmol/L per ms
I_{tr}	Ca^{2+} transfer from NSR to JSR,	mmol/L per ms
$I_{diff,x}$	Ionic diffusion of Ca^{2+}, Cl^{-} or Na^{+} from SR subspace to myoplasm	
$CaMK_{bound}$	Fraction of CaMKII binding sites bound to Ca^{2+} / calmodulin	
$CaMK_{active}$	Fraction of active CaMKII binding sites	
$CaMK_{trap}$	Fraction of autonomous CaMKII binding sites with trapped calmodulin	
$CaMK_{o}$	Equilibrium fraction of active CaMKII binding sites, 0.05	
α_{CaMK}	Phosphorylation rate of CaMKII,0.5	ms^{-1}
β_{CaMK}	Dephosphorylation rate of CaMKII, 0.00068	ms^{-1}
$\bar{\Delta}P$	Maximal CaMKII-dependent change in parameter P	
ΔP_{CaMK}	CaMKII-dependent factor of substrate parameter P	
$K_{m,CaM}$	CaMK half-saturation coefficient, 0.0015	mmol/L
$K_{m,CaMK}$	Half-saturation coefficient of substrate parameter, 0.15	
β_0	I_{rel} , minimal value of β_τ, 4.75	ms
$\Delta\beta_0$	I_{rel} , I rel , Maximal CaMK dependent change for β_τ, 1	mmol/L
K_β	I_{rel} , half saturation coefficient for $\Delta\beta_{\tau,CaMK}$,0.28	mmol/L
$K_{Rel,\infty}$	I_{rel} , half saturation coefficient for $I_{rel,\infty}$,1	mmol/L
h_{Rel}	I_{rel} , Hill coefficient for $I_{rel,\infty}$,8	
h_β	I_{rel} , Hill coefficient for $\Delta\beta_{\tau,CaMK}$,10	
κ	I_{rel} , Amplitude coefficient for α_{Rel},0.1125	$\mu A/\mu F$
$K_{Rel,\tau}$	I_{rel} , Half saturation coefficient for $I_{Rel,\tau}$, 0.0123	mmol/L
$\bar{\Delta}K_{m,PLB}$	I_{up} , Phospholamban Half-saturation factor, 1.7 $\times 10^{-4}$	mmol/L
$\bar{\Delta}I_{up,CaMK}$	I_{up} , Maximal CaMK dependent change in I_{up}, 0.75	
$\bar{I}_{up}$	I_{up} , Maximal value of I_{up}, 0.004375	mmol/L per ms
$K_{m,up}$	I_{up} , Half saturation of I_{up}, 0.000925	mmol/L
τ_{tr}	I_{tr}, Time constant for NSR/JSR Ca^{2+} transfer, 25	ms

$I_{Na,b}$ is not included in the HRd model due to the presence of CT_{NaCl} , which brings Na^{+} into the cell at rest. $I_{Ca,K}$ and $I_{Ca,Na}$ are assumed to be insignificant and are eliminated from the HRd model.

Table 5: **Concentrations and Buffering**

$[Ca^{2+}]_x$	Calcium concentration in compartment X	mmol/L
$[Na^{+}]_x$	Sodium concentration in compartment X	mmol/L
$[K^{+}]_x$	Potassium concentration in compartment X	mmol/L
$[Cl^{-}]_x$	Chloride concentration in compartment X	mmol/L
csqn	Calsequestrin, Ca^{2+} buffer in JSR	
trpn	Troponin,Ca^{2+} buffer in myoplasm	
cmdn	Calmodulin,Ca^{2+} buffer in myoplasm	
BSR_X	Anionic SR binding sites for Ca^{2+} (SS or SS,CaL)	
BSL_X	Anionic sarcolemmal binding sites for Ca^{2+} (SS or SS,CaL)	
$\overline{[trpn]}$	Maximum troponin concentration, 0.07	mmol/L
$\overline{[cmdn]}$	Maximum calmodulin concentration, 0.05	mmol/L
$K_{m,cmdn}$	Calmodulin half saturation, 0.00238	mmol/L
$K_{m,trpn}$	Troponin half saturation, 0.0005	mmol/L
$\overline{[csqn]}$	Calsequestrin concentration, 10.0	mmol/L
$K_{m,csqn}$	Calsequestrin half saturation, 0.8	mmol/L

Table 6: **Compartments**

i	intracellular space
o	extracellular space
SR	sarcoplasmic reticulum
JSR	junctional sarcoplasmic reticulum
NSR	network sarcoplasmic reticulum
SS,SR	SR Ca_{2+} release subspace
SS,CaL	L-type Ca_{2+} entry subspace

CaMKII

$$
\begin{aligned}
CaMK_{bound} &= CaMK_0.\,(1 - CaMK_{trap}).\left(\frac{1}{1+\frac{K_{mCaM}}{[Ca^{2+}]_{SS}}}\right) \\
\frac{dCaMK_{trap}}{dt} &= \alpha_{CaMK}.\,CaMK_{bound}.\,(CaMK_{bound} + CaMK_{trap}) \\
&\quad -\beta_{CaMK}.CaMK_{trap} \\
CaMK_{active} &= CaMK_{bound} + CaMK_{trap} \\
\text{where} & \\
\alpha_{CaMK} &= 0.05\ ms^{-1} \\
\beta_{CaMK} &= 0.00068\ ms^{-1} \\
CaMK_0 &= 0.05 \\
K_{mCaM} &= 0.0015\ mmol/L
\end{aligned}
$$

Table 7: **External Concentrations (Single cell)**

$[Ca^{2+}]_o$	1.8	mmol/L
$[Cl^-]_o$	100	mmol/L
$[K^+]_o$	5.4	mmol/L
$[Na^+]_o$	140	mmol/L

Table 8: **Resting voltage and concentrations (Single cell)**

V_m	-87.472528	mV
$[Ca^{2+}]_i$	0.0000822	mmol/L
$[Ca^{2+}]_{SS,SR}$	0.000138151	mmol/L
$[Ca^{2+}]_{SS,CaL}$	0.000143898	mmol/L
$[Ca^{2+}]_{JSR}$	1.25	mmol/L
$[Ca^{2+}]_{NSR}$	1.25	mmol/L
$[Cl^-]_i$	19.53	mmol/L
$[Cl^-]_{SS}$	20.26905	mmol/L
$[K^+]_i$	142.82	mmol/L
$[Na^+]_i$	9.71	mmol/L
$[Na^+]_{SS}$	6.935607	mmol/L

I_{CaL}

$$
\begin{aligned}
I_{CaL} &= d^{pow}.\, f_{ca}.\, f_{ca2}.\, f.\, f_2.\, \bar{I}_{CaL} \\
\bar{I}_{CaL} &= P_{Ca}.\, z_{Ca}^2.\, \frac{(V_m - 15.0).F^2}{RT} \\
&\quad .\frac{\gamma_{Cai}.[Ca]_{SS}.\exp\left(z_{Ca}.(Vm - 15.0).\frac{F}{RT}\right)i - \gamma_{Cao}.[Ca]_o}{\exp\left(z_{Ca}.(V_m - 15.0).\frac{F}{RT}\right) - 1} \\
d_\infty &= \frac{1}{1 + \exp\left(-\frac{(V_m - 4)}{6.74}\right)} \\
\tau_d &= 0.59 + 0.8.\, \frac{\exp\left((0.052.(V_m + 13))\right)}{1 + \exp\left((0.132.(V_m + 13))\right)} \\
pow_\infty &= 9 - \frac{8}{1 + \exp\left(\frac{-(V_m + 65)}{3.4}\right)} \\
f_\infty &= \frac{0.7}{1.0 + \exp\left(\frac{V_m + 17.12}{7}\right)} + 0.3 \\
f_{2\infty} &= \frac{0.77}{1.0 + \exp\left(\frac{V_m + 17.12}{7}\right)} + 0.23 \\
\tau_f &= \frac{1}{0.2411.\exp\left(-[0.045.(V_m - 9.6914)]^2\right) + 0.0529} \\
\tau_{f2} &= \frac{1}{0.0423.\exp\left(-[0.059.(V_m - 18.5729)]^2\right)} \\
f_{Ca\infty} &= \frac{0.3}{1 - \frac{I_{CaL}}{0.05}} + \frac{0.55}{1 + 12\frac{[Ca^{2+}]_{SS}}{0.003}} + 0.15 \\
f_{Ca2\infty} &= \frac{1}{1 - \frac{I_{CaL}}{0.01}} \\
\Delta\tau_{fcaCaMK} &= \overline{\Delta}\tau_{fcaCaMK} \cdot \frac{CaMK_{active}}{K_{mCaMK} + CaMK_{active}} \\
\tau_{fca} &= \Delta\tau_{fcaCaMK} + 0.5 + \frac{1}{1.0 + \frac{[Ca^{2+}]_{SS}}{0.003}}\, ms
\end{aligned}
$$

Table 9: **Cell Geometry**

Length (L)	0.01	cm
Cell volume, $V_{cell} = \pi.r^2.L$	38×10^{-6}	μL
Geometric membrane area: $A_{geo} = 2\pi r^2 + 2\pi rL$	0.767×10^{-4}	cm^2
Capacitative membrane area: $A_{cap} = R_{CG}.A_{geo}$	1.534×10^{-4}	cm^2
Myoplasmic volume, $V_{myo} = V_{cell}.68\%$	25.84×10^{-6}	μL
Mitochondrial volume, $V_{mito} = V_{cell}.26\%$	9.88×10^{-6}	μL
SR volume, $V_{SR} = V_{cell}.6\%$	2.28×10^{-6}	μL
NSR volume, $V_{NSR} = V_{cell}.5.52\%$	2.098×10^{-6}	μL
JSR volume, $V_{JSR} = V_{cell}.0.48\%$	0.182×10^{-6}	μL
SS,SR volume, $V_{SS,SR} = V_{cell}.2.0\%$	0.76×10^{-6}	μL
SS,CaL volume, $V_{SS,CaL} = V_{cell}.0.2\%$	0.076×10^{-6}	μL

I_{Ks}

$$
\begin{aligned}
I_{Ks} &= \overline{G}_{Ks}.X_s.X_{s2}.(Vm - E_{Ks}) \\
\overline{G}_{Ks} &= 0.0248975\left(1 + \frac{0.6}{1 + \left[\frac{3.8\times10^{-5}}{[Ca^{2+}]_i}\right]^{1.4}}\right) \\
E_{Ks} &= \frac{RT}{F}.\ln\left(\frac{[K^+]_o + P_{NaK}.[Na^+]_o}{]K^+]_i + P_{NaK}.[Na^+]_i}\right) \\
X_{s\infty} &= X_{s2\infty} = \frac{1}{1 + \exp\left(\frac{-(V_m - 10.5)}{24.7}\right)} \\
\tau_{xs1} &= \frac{1}{\left[\frac{7.61\times10^{-5}.(V_m+44.6)}{1-\exp(-9.97.(V_m+44.6))}\right] + \left[\frac{3.6\times10^{-4}.(V_m-0.55)}{\exp(0.128.(V_m-0.55))-1}\right]} \\
\tau_{xs2} &= 2.\tau_{xs1} \\
\text{where} & \\
P_{NaK} &= 0.01833
\end{aligned}
$$

I_{Kr}

$$
\begin{aligned}
I_{Kr} &= \overline{G}_{Kr}.X_r.R_{Kr}.(V_m - E_{Kr}) \\
\overline{G}_{Kr} &= 0.0138542.\sqrt{\frac{[K^+]_o}{5.4}} \\
E_{Kr} &= \frac{RT}{F}.\ln\left[\frac{[K^+]_0}{[K^+]_i}\right] \\
\tau_{Xr} &= \frac{1}{\left[\frac{0.6\times10^{-3}.(V_m-1.7384)}{1-\exp(-0.136.(V_m-1.7384))}\right] + \left[\frac{3\times10^{-4}.(V_m+38.3608)}{\exp(0.1522.(V_m+38.3608))-1}\right]} \\
R_{Kr} &= \frac{1}{1+\exp\left(\frac{V_m+10}{15.4}\right)}
\end{aligned}
$$

I_{to1}

$$
\begin{aligned}
I_{to1} &= \overline{G}_{to1}.a^3.i.i_2.R_{to1}.(V_m - E_{to1}) \\
E_{to1} &= \frac{RT}{F}.\ln\left(\frac{[K^+]_o}{[K^+]_o}\right) \\
R_{to1} &= \exp\left(\frac{V_m}{300}\right) \\
\alpha_a &= \frac{25.\exp\left(\frac{(V_m-40}{25}\right)}{1+\exp\left(\frac{(V_m-40}{25}\right)} \\
\beta_a &= \frac{25.\exp\left(\frac{-(V_m+90}{25}\right)}{1+\exp\left(\frac{(-V_m+90}{25}\right)} \\
\alpha_i &= \frac{0.03}{1+\exp\left(\frac{(V_m+60}{5}\right)} \\
\beta_i &= \frac{0.2.\exp\left(\frac{(V_m+25}{5}\right)}{1+\exp\left(\frac{(V_m+25}{5}\right)} \\
\alpha_{i2} &= \frac{0.00225}{1+\exp\left(\frac{(V_m+60}{5}\right)} \\
\beta_{i2} &= \frac{0.1.\exp\left(\frac{(V_m+25}{5}\right)}{1+\exp\left(\frac{(V_m+25}{5}\right)} \\
\text{where} & \\
\overline{G}_{to1} &= 0.19\ mS/\mu F
\end{aligned}
$$

$\mathbf{I_{NaCa}}$

$$
\begin{aligned}
I_{NaCa} &= Allo.\Delta E \\
Allo &= \frac{1}{1+\left(\frac{K_{mCa,act}}{1.5.[Ca^{2+}]_i}\right)^2} \\
\Delta E &= \frac{\nu_{max}.\left([Na^+]_i{}^3.[Ca^{2+}]_o.\ \exp\left(\eta.\frac{VF}{RT}\right)-[Na^+]_o{}^3.1.5.[Ca^{2+}]_i.\ \exp\left(\frac{(\eta-1).VF}{RT}\right)\right)}{\left(\begin{array}{l}\left(1+k_{sat}\exp\left(\frac{\eta-1).VF}{RT}\right)\right)\ . \\ \left(K_{mCao}[Na^+]_i{}^3+K^3_{mNao}.1.5.[Ca^{2+}]_i+K^3_{mNai}.[Ca^{2+}]_o.\left(1+\frac{1.5.[Ca^{2+}]_i}{K_{mCai}}\right)\right) \\ +\left(K_{mCai}.[Na^+]^3_o.\left(1+\frac{[Na^+]^3_o}{K^3_{mNai}}\right)+[Na^+]^3_i.[Ca^{2+}]_o+[Na^+]^3_o.1.5.[Ca^{2+}]_i\right)\end{array}\right)}
\end{aligned}
$$

where

$$
\begin{aligned}
\nu_{max} &= 4.5\ \mu A/\mu F \\
k_{sat} &= 0.27 \\
\eta &= 0.35 \\
K_{mNai} &= 12.3\ mmol/L \\
K_{mNao} &= 87.5\ mmol/L \\
K_{mCai} &= 0.0036\ mmol/L \\
K_{mCao} &= 1.3\ mmol/L \\
K_{mCa,act} &= 1.25\times 10^{-4}\ mmol/L
\end{aligned}
$$

$\mathbf{I_{Na}}$

$$
\begin{aligned}
I_{Na} &= \overline{G}_{Na}.\, m^3.\, h.j\,.\,(V_m - E_{Na}) \\
\overline{G}_{Na} &= 8.25\, mS/\mu F \\
E_{Na} &= \frac{RT}{F}.\ \ln\left(\frac{[Na^+]_o}{[Na^+]_i}\right) \\
\alpha_m &= \frac{0.32\,.(V_m + 47.13)}{1 - \exp\,(V_m + 47.13)} \\
\beta_m &= 0.08.\ \exp\left(-\frac{V_m}{11}\right)
\end{aligned}
$$

$$
\begin{aligned}
\text{If}\quad V_m &\geq -40.0\, mV, \\
\alpha_h &= 0.0 \\
\beta_h &= \frac{1}{0.13.\ \left(1 + \exp\left(\frac{(V_m + 10.66)}{-11.1}\right)\right)} \\
\alpha_j &= 0.0 \\
\beta_j &= \frac{0.3\exp\left(-2.535 \times 10^{-7}.V_m\right)}{1 + \exp\left(-0.1.(V_m + 32)\right)}
\end{aligned}
$$

else

$$
\begin{aligned}
\alpha_h &= 0.135.\ \exp\left(\frac{(80.0 + V_m}{-6.8}\right) \\
\beta_h &= 3.56.\ \exp\left(0.079.V_m\right) + 3.1 \times 10^5.\ \exp\left(0.35.V_m\right) \\
\alpha_j &= (V_m + 37.78)\,.\left[\frac{\left(-1.2714 \times 10^5.\exp\left(0.2444.V_m\right) - 3.474 \times 10^{-5}.\exp\left(-0.04391.V_m\right)\right)}{1 + \exp\,(0.311.(V_m + 79.23))}\right] \\
\beta_j &= \frac{0.1212.\exp\left(-0.01052.V_m\right)}{1 + \exp\,(-0.1378.(V_m + 40.14))}
\end{aligned}
$$

I_{NaL}

$$
\begin{aligned}
I_{NaL} &= \overline{G}_{NaL} \,.{m_L}^3.\, h_L\, (V_m - E_{NaL}) \\
E_{NaL} &= \frac{RT}{F}.\ \ln\left(\frac{[Na^+]_o}{[Na^+]_i}\right) \\
\alpha_{mL} &= \frac{0.32\,.(V_m + 47.13)}{1 - \exp\,(V_m + 47.13)} \\
\beta_{mL} &= 0.08.\ \exp\left(-\frac{V_m}{11}\right) \\
h_{L\infty} &= \frac{1}{1 + \exp\left(\frac{V_m + 91}{6.1}\right)} \\
\text{where} & \\
\overline{G}_{NaL} &= 0.0065\, mS/\mu F \\
\tau_{hL} &= 600\, ms
\end{aligned}
$$

Cl⁻ Currents

$$
\begin{aligned}
E_{Cl} &= -\frac{RT}{F}.\ \ln\left(\frac{[Cl^-]_o}{[Cl^-]_i}\right) \\
E_K &= \frac{RT}{F}.\ \ln\left(\frac{[K^+]_o}{[K^+]_i}\right) \\
E_{Na} &= \frac{RT}{F}.\ \ln\left(\frac{[Na^+]_o}{[Na^+]_i}\right)
\end{aligned}
$$

CT_{KCl}, K^+–Cl^- Cotransporter

$$
\begin{aligned}
CT_{KCl} &= \overline{CT}_{KCl}.\ \frac{(E_K - E_{Cl})}{(E_K - E_{Cl}) + 87.8251^4} \\
\overline{CT}_{KCl} &= 7.0756 \times 10^{-6}\ mmol/L\ per\ ms
\end{aligned}
$$

CT_{NaCl}, Na^+–Cl^- Cotransporter

$$
\begin{aligned}
CT_{NaCl} &= \overline{CT}_{NaCl}.\ \frac{(E_{Na} - E_{Cl})^4}{(E_{Na-}E_{Cl})^4 + 87.8251} \\
\overline{CT}_{NaCl} &= 9.8443 \times 10^{-6}\ mmol/L\ per\ ms
\end{aligned}
$$

I_{Clb}, Cl^- background current

$$
\begin{aligned}
I_{Clb} &= \overline{G}_{Clb}.\left(V_m - E_{Cl}\right) \\
\overline{G}_{Clb} &= 2.25 \times 10^{-4}\ \mu A/\mu F
\end{aligned}
$$

I_{to2}, Ca^{2+}-dependent transient outward current

$$
\begin{aligned}
\bar{I}_{to2} &= P_{Cl}.z_{Cl}^2.\frac{V_m.F^2}{RT}.\frac{\left([Cl^-]_i - [Cl^-]_o\right).\ \exp\left(-z_{Cl}.V_m.\frac{F}{RT}\right)}{1 - \exp\left(-z_{Cl}.V_m.\frac{F}{RT}\right)} \\
aa_\infty &= \frac{1}{1 + \frac{K_{mto2}}{[Ca^{2+}]_r}} \\
\text{where} & \\
\tau_{aa} &= 1\ ms \\
P_{Cl} &= 4.0 \times 10^{-7}\ cm/s \\
K_{mto2} &= 0.1502\ mM \\
Ito1 &= \bar{I}_{to2}\ .\ aa
\end{aligned}
$$

I_{rel}

$$
\begin{aligned}
I_{rel} &= \overline{G}_{rel}.\, ro.\, ri.\left([Ca^{2+}]_{JSR} - [Ca^{2+}]_{SS}\right) \\
\overline{G}_{rel} &= 3000.vg\ ms^{-1} \\
vg &= \frac{1}{1+\exp\left(\frac{\bar{I}_{CaL}+13}{5}\right)} \\
\tau_{ri} &= \frac{350 - \Delta\tau_{relCaMK}}{1+\exp\left(\frac{[Ca^{2+}]_{SS}-0.003+0.003.\, cafac}{0.0002}\right)} + 3 + \Delta\tau_{rel,CaMK}\ ms \\
ri_{\infty} &= \frac{1}{1+\exp\left(\frac{[Ca^{2+}]_{SS}-0.0004+0.002.\, cafac}{000025}\right)} \\
cafac &= \frac{1}{1+\exp\left(\frac{I_{CaL}+0.05}{0.015}\right)} \\
ro_{\infty} &= \frac{{I_{CaL}}^2}{{I_{CaL}}^2 + 1.0^2}.\, \Delta ro_{\infty,JSR} \\
\Delta ro_{\infty,JSR} &= \frac{{[Ca^{2+}]_{JSR}}^{1.9}}{{[Ca^{2+}]_{JSR}}^{1.9} + \left[\frac{49.28.[Ca^{2+}]_{SS}}{[Ca^{2+}]_{SS}+0.0028}\right]^{1.9}} \\
\Delta\tau_{rel,CaMK} &= \overline{\Delta\tau}_{ral,CaMK}.\frac{CaMK_{active}}{K_{mCaMK} + CaMK_{active}} \\
\text{where} & \\
\overline{\Delta\tau}_{rel,CaMK} &= 10\ ms \\
\tau_{ro} &= 3\ ms \\
K_{mCaMK} &= 0.15
\end{aligned}
$$

SR Fluxes

I_{up}

$$
\begin{aligned}
I_{up} &= \left(\Delta I_{up,CaMK} + 1\right).\bar{I}_{up}.\frac{[Ca^{2+}]_i}{[Ca^{2+}]_i + K_{m,up} - \Delta K_{m,PLB}} \\
\Delta I_{up,CaMK} &= \overline{\Delta I}_{up,CaMK}.\frac{CaMK_{active}}{K_{mCaMK} + CaMKactive} \\
\Delta K_{m,PLB} &= \overline{\Delta K}_{m,PLB}.\frac{CaMK_{active}}{K_{mCaMK} + CaMKactive} \\
\text{where} & \\
\overline{\Delta K}_{m,PLB} &= 0.00017\ mmol/L \\
\overline{\Delta I}_{up,CaMK} &= 0.75\ mmol/L \\
K_{mCaMK} &= 0.15 \\
\bar{I}_{up} &= 0.004375\ mmol/L\ per\ ms \\
K_{m,up} &= 0.00092\ mmol/L
\end{aligned}
$$

I_{leak}

$$
\begin{aligned}
I_{leak} &= \frac{0.004375}{\overline{NSR}}.\ [Ca^{2+}]_{NSR} \\
\text{where} & \\
\overline{NSR} &= 15\ mmol/L
\end{aligned}
$$

I_{tr}

$$
\begin{aligned}
I_{tr} &= \frac{[Ca^{2+}]_{NSR} - [Ca^{2+}]_{JSR}}{\tau_{tr}} \\
\text{where} & \\
\tau_{tr} &= 120\ ms
\end{aligned}
$$

Calcium Buffers

Ca^{2+} buffers in myoplasm

$$
\begin{aligned}
Buffered[trpn] &= [\overline{trpn}].\frac{[Ca^{2+}]_i}{[Ca^{2+}]_i + K_{mtrpn}} \\
Buffered[cmdn] &= [\overline{cmdn}].\frac{[Ca^{2+}]_i}{[Ca^{2+}]_i + K_{mcmdn}} \\
\text{where} & \\
\overline{[trpn]} &= 0.07\ mmol/L \\
\overline{[cmdn]} &= 0.05\ mmol/L \\
K_{mtrpn} &= 0.0005\ mmol/L \\
K_{mcmdn} &= 0.00238\ mmol/L
\end{aligned}
$$

Ca^{2+} buffer in JSR

$$
\begin{aligned}
Buffered[csqn] &= [\overline{csqn}].\frac{[Ca^{2+}]_{JSR}}{[Ca^{2+}]_{JSR} + K_{mcsqn}} \\
\text{where} & \\
\overline{[csqn]} &= 0.07\ mmol/L \\
K_{mcsqn} &= 0.0005\ mmol/L
\end{aligned}
$$

Time Independent Currents

I_{Cab}

$$
\begin{aligned}
I_{Cab} &= P_{Cab}.\ z_{Ca}^2.\ \frac{V_m.F^2}{RT}.\frac{\gamma_{Cai}.[Ca^{2+}]_i.\exp\left(z_{ca}.V_m.\frac{F}{RT}\right) - \gamma_{Cao}.[Ca]_o}{\exp\left(z_{Ca}.V_m.\frac{F}{RT}\right) - 1} \\
\text{where} & \\
P_{Cab} &= 1.995084 \times 10^{-7}\ cm/s \\
\gamma_{Cai} &= 1 \\
\gamma_{Cao} &= 0.341
\end{aligned}
$$

I_{NaK}

$$
\begin{aligned}
I_{NaK} &= \overline{G}_{NaK}.\frac{f_{NaK}}{1+\left(\frac{K_{mNai}}{[Na^+]_i}\right)^2}.\left(\frac{[K^+]_o}{[K^+]_o+K_{mKo}}\right)\\
f_{NaK} &= \frac{1}{1+0.1245.\exp\left(\frac{-0.1.V_m.F}{RT}\right)+0.0365.\sigma.\exp\left(\frac{-V_m.F}{RT}\right)}\\
\sigma &= \frac{\exp\left(\frac{[Na^+]_o}{67.3}\right)-1.0}{7.0}\\
\text{where}&\\
\overline{G}_{NaK} &= 0.61875\ mS/\mu F\\
K_{mNai} &= 10\ mM\\
K_{mKo} &= 1.5\ mM
\end{aligned}
$$

I_{Kp}

$$
\begin{aligned}
I_{Kp} &= \overline{G}_{Kp}.K_p.\left(V_m-E_{Kp}\right)\\
K_p &= \frac{1}{1+\exp\left(\frac{7.488-V_m}{5.98}\right)}\\
E_{Kp} &= \frac{RT}{F}.\ln\left(\frac{[K^+]_o}{[K^+]_i}\right)\\
\text{where}&\\
\overline{G}_{Kp} &= 2.76\times10^{-3}\ mS/\mu F
\end{aligned}
$$

I_{K1}

$$
\begin{aligned}
I_{K1} &= \overline{G}_{K1}.K_1.\left(V_m-E_{K1}\right)\\
\overline{G}_{K1} &= 0.5.\sqrt{\frac{[K^+]_o}{5.4}}\ mS/\mu F\\
K_1 &= \frac{\alpha_{K1}}{\alpha_{K1}+\beta_{K1}}\\
\beta_{K1} &= \frac{0.49124.\exp\left(0.08032.(V_m-E_{K1}+5.476)\right)+\exp\left(0.06175.(V_m-E_{K1}-594.31)\right)}{1+\exp\left(-0.5143.(V_m-E_{K1}+4.753)\right)}\\
\alpha_{K1} &= \frac{1.02}{1+\exp\left(0.2385.(V_m-E_{K1}-59.215)\right)}\\
E_{K1} &= \frac{RT}{F}.\ln\left(\frac{[K^+]_o}{[K^+]_i}\right)
\end{aligned}
$$

I_{pCa}

$$
\begin{aligned}
I_{pCa} &= \overline{G}_{pCa}.\frac{[Ca^{2+}]_i}{[Ca^{2+}]_i + K_{mpCa}} \\
\text{where} & \\
\overline{G}_{pCa} &= 0.0575\ mS/\mu F \\
K_{mpCa} &= 0.0005\ mM
\end{aligned}
$$

Ion concentrations

Intracellular ion concentrations

Ca^{2+}

$$
\begin{aligned}
\frac{d[Ca^{2+}]_i}{dt} &= -\left(I_{Cab} + I_{pCa} - 2.I_{NaCa}.\frac{A_{Cap}}{V_{myo}.2F} + (I_{up} - I_{leak}).\frac{V_{NSR}}{V_{myo}} - I_{Diff}.\frac{V_{SS}}{V_{myo}}\right) \\
[Ca^{2+}]_{it} &= [trpn] + [cmdn] + [Ca^{2+}]_i + \Delta[Ca^{2+}]_i \\
[Ca^{2+}]_i &= \frac{2}{3}.\sqrt{b^2 - 3c}\ cos\left(\frac{1}{3}cos^{-1}\left(\frac{9bc - 2b^3 - 27d}{2(b^2 - 3c)^{1.5}}\right)\right) - \frac{b}{3} \\
b &= [\overline{trpn}] + [\overline{cmdn}] - [Ca^{2+}]_{it} + K_{mcmdn} + K_{mtrpn} \\
c &= K_{mcmdn}.K_{mtrpn} - [Ca^{2+}]_{it}.\left(K_{mtrpn} + K_{mcmdn}\right) + [\overline{trpn}]. \\
& \quad K_{mcmdn} + [\overline{cmdn}].K_{mtrpn} \\
d &= -K_{mtrpn}.K_{mcmdn}.[Ca^{2+}]_{it}
\end{aligned}
$$

Na^+

$$
\frac{d[Na^+]_i}{dt} = -I_{Nat}.\frac{A_{Cap}}{V_{myo}.F} + CT_{NaCl}
$$

K^+

$$
\frac{d[K^+]_i}{dt} = -I_{Kt}.\frac{A_{Cap}}{V_{myo}.F} + CT_{KCl}
$$

Cl^-

$$
\frac{d[Cl^-]_i}{dt} = I_{Clt}.\frac{A_{Cap}}{V_{myo}.F} + CT_{NaCl} + CT_{KCl}
$$

SR calcium concentrations
JSR

$$\begin{aligned}
\frac{d[Ca^{2+}]_{JSR}}{dt} &= I_{tr} - I_{rel} \\
[Ca^{2+}]_{JSR} &= \frac{\sqrt{b^2 + 4c} - b}{2} \\
b &= [\overline{csqn}] - [csqn] - [Ca^{2+}]_{JSR} - \Delta[Ca^{2+}]_{JSR} + K_{mcsqn} \\
c &= K_{mcsqn}.\left([csqn] + [Ca^{2+}]_{JSR} + \Delta[Ca^{2+}]_{JSR}\right)
\end{aligned}$$

NSR

$$\frac{d[Ca^{2+}]_{NSR}}{dt} = I_{up} - I_{leak} - I_{tr}.\frac{V_{JSR}}{V_{NSR}}$$

Subspace calcium concentration

$$\begin{aligned}
\frac{d[Ca^{2+}]_{SS}}{dt} &= \beta_{SS}.\left(-I_{Ca}.\frac{A_{Cap}}{V_{SS}.2F} + Irel.\frac{V_{JSR}}{V_{SS}} - I_{Diff}\right) \\
I_{Diff} &= \frac{[Ca^{2+}]_{SS} - [Ca^{2+}]_i}{\tau_{Diff}} \\
\beta_{SS} &= \frac{1}{1 + \frac{\overline{BSR}.K_{mBSR}}{(K_{mBSR}+[Ca^{2+}]_{SS})^2} + \frac{\overline{BSL}.K_{mBSL}}{(K_{mBSL}+[Ca^{2+}]_{SS})^2}} \\
\text{where} & \\
\tau_{Diff} &= 0.2\ cm \\
\overline{BSR} &= 0.047\ mM \\
K_{mBSR} &= 0.00087\ mM \\
\overline{BSL} &= 1.124 mM \\
K_{mBSL} &= 0.0087 mM
\end{aligned}$$

The total transmembrane current at time t
Total transmembrane Ca^{2+} current
$I_{Cat} = I_{CaL} + I_{Cab} + I_{pCa} - 2I_{NaCa}$

Total transmembrane Na^{+} current
$I_{Nat} = I_{Na} + 3I_{NaK} + I_{CaNa} + I_{NaL}$

Total transmembrane K^{+} current
$IKt = I_{Ks} + I_{Kr} + I_{K1} + I_{CaK} + I_{to1} + I_{Kp} - 2I_{NaK}$

Total transmembrane Cl^- current

$I_{Clt} = I_{to2} + I_{Clb}$

Total transmembrane current

$I_{tot} = I_{Cat} + I_{Nat} + I_{Kt} + I_{Clt}$

Conservative current stimulus,I_{stim}

$$I_{Kt} = I_{Kt} + 0.5.I_{stim} I_{Clt} = I_{Clt} + 0.5.I_{stim}$$

Transmembrane voltage, V_m

$\frac{dV_m}{dt} = \frac{-I_{tot}}{C_m}$

Electrical Wave Propagation in Cardiac Tissue

In a cardiac-tissue mathematical model, the time evolution of the transmembrane voltage is given by a partial differential equation (PDE) of the reaction-diffusion type:

$$\frac{\partial V}{\partial t} = \nabla.\mathcal{D}\nabla V - \frac{I_{ion} + I_{applied}}{C_m}, \tag{7}$$

where I_{ion} contains all the ionic currents, $I_{applied}$ is the external current, C_m the capacitance density, and $\mathcal{D}$ the diffusion tensor that accounts for the conductivity of the tissue and propagation between cells; its elements are described by:

$$\mathcal{D}_{ij} = D_T * \delta_{ij} + (D_L - D_T)\alpha_i\alpha_j. \tag{8}$$

Here, α_is are the components of α, the unit vector along the direction of the local muscle fiber. We solve the PDE for V by a finite-difference scheme. Table 10 contains a list of the currents in the HRD model and their descriptions.

[1] F.H. Fenton, E.M. Cherry, A. Karma, and W.J. Rappel, CHAOS **15**, 013502 (2005)

Table 10: Table showing all the major currents in the HRD model and their descriptions. The units for all the currents are $\mu A/\mu F$.

Current	Description
I_{Na}	Fast Na^+ current
I_{NaL}	Slowly inactivating late Na^+ current
I_{CaL}	Ca^{2+} current through the L-type Ca^{2+} channel
I_{NaCa}	Na^+ -Ca^2+ exchanger
I_{NaK}	$Na^+ - K^+$ pump
I_{Kr}	Rapid delayed rectifier K^+ current
I_{Ks}	Slow delayed rectifier K^+ current
I_{to1}	4AP-sensitive transient outward K^+ current
I_{to2}	Ca^{2+} -dependent transient outward Cl^- current
I_{K1}	Time-independent K^+ current
I_{Kp}	Plateau K^+ current
I_{Cab}	Background Ca^{2+} current
I_{Clb}	background Cl^- current
I_{IpCa}	Sarcolemmal Ca^{2+} pump
I_{rel}	Ca^{2+} release from JSR to myoplasm